

Emissivity Simulations in Passive Microwave Remote Sensing With 3-D Numerical Solutions of Maxwell Equations

Lin Zhou, Leung Tsang, *Fellow, IEEE*, Vikram Jandhyala, Qin Li, and C. H. Chan, *Fellow, IEEE*

Abstract—In the numerical Maxwell-equation model (NMM3D) of rough-surface scattering, we solve Maxwell equations in three dimensions to calculate emissivities for applications in passive microwave remote sensing of soil and ocean surfaces. The difficult cases for soil surfaces are with exponential correlation functions when the surfaces have fine-scale structures of large slopes. The difficulty for ocean surfaces is that because the emissivities are close to that of a flat surface, the emissivities have to be calculated accurately to correctly assess the rough-surface effects. In this paper, the accuracies of emissivity calculations are improved by using Rao–Wilton–Glisson basis functions. We further use sparse matrix canonical method to solve the matrix equation of Poggio–Miller–Chang–Harrington–Wu integral equations. Energy conservation checks are provided for the simulations. Comparisons are made with results from the pulse basis function. Numerical results are illustrated for soil and ocean surfaces respectively with exponential correlation function and ocean spectrum. The emissivities of soil are illustrated at both L- and C-bands and at multiple incidence angles for the same physical roughness parameters. The brightness temperatures for ocean surfaces are illustrated for cases with various wind speeds. We compare results with those from the sparse matrix methods. Comparisons are also made with experimental emissivity measurements of soil surfaces. Parallel computation is also implemented. Lookup tables of emissivities based on NMM3D are provided.

Index Terms—Electromagnetic scattering, integral equations, microwave remote sensing, rough surface, Rao–Wilton–Glisson (RWG), sparse-matrix canonical-grid (SMCG).

I. INTRODUCTION

THERE is an increasing interest in simulating electromagnetic scattering from rough surfaces with applications in active and passive microwave remote sensing of soil, ocean, and ice, etc. The small perturbation method (SPM) and Kirchhoff approximation are classical theories of wave scattering of rough surfaces. They are limited in regimes of validity [1], [2] and do not give the correct frequency and polarimetric dependence. With the advent of modern computers and fast

computation methods, numerical simulations for rough-surface scattering have become attractive. The common methods are the fast multipole method (FMM) [3], [4] and the sparse-matrix canonical-grid (SMCG) method [5]–[8]. The computational complexity and memory requirement of FMM and SMCG are $O(N)$ and $O(N \log N)$, respectively. However, most numerical simulations are concerned with radar active remote sensing [9]–[12]. There is less work on simulations for passive remote sensing. A reason is that the accuracy requirement of passive remote sensing is stringent [13]. Some numerical methods can give good results in active remote sensing, which calculate bistatic coefficients in decibel scale, and give poor results in passive remote sensing, which calculates emissivity as a fraction. The difficult cases for soil surfaces are with exponential correlation functions when surfaces have fine-scale structures of large slopes. The difficulty for ocean surfaces is that because the emissivities are close to that of a flat surface, the emissivities have to be calculated accurately to correctly assess the rough-surface effects.

Over the last few years, we have made significant progress on the SMCG method for solving large-scale random rough-surface scattering problems. Results up to six million boundary unknowns have been reported [14]–[16]. In the method, we use a decomposition of the impedance matrix into strong near-field interaction and weak far-field interaction matrices. The far interactions, which require large CPU, can be computed simultaneously through fast Fourier transforms (FFTs) by making Taylor series expansions of the Green's functions about a uniformly spaced canonical grid. The original version of the sparse matrix canonical-grid method was developed with the pulse basis function and point matching method [7], [8], [17].

Using the pulse basis functions method and combined with SMCG, researchers have applied to simulations of emissivities in passive microwave remote sensing. Johnson *et al.* [18] studied the case of ocean emissivity at nadir incidence using eight points per wavelengths. The accuracy of the impedance matrix elements was attained by using large order of integration quadrature. Later, it was found that in order to have better accuracy, a dense discretization is needed for the Green's function of the dielectric medium. The physics-based two-grid (PBTG) method was developed such that the dense sampling is used and yet the CPU and memory requirements remain comparable to that of coarser sampling. The SMCG/PBTG method was used to study emissivity of soil surface which was assumed to be a Gaussian random process with a Gaussian correlation function [7], [8], [17]. The results were compared

Manuscript received June 5, 2004; revised April 6, 2004. This work was supported in part by the Office of Naval Research under Grant N00014-99-1-0190 to the University of Washington and in part by the City University of Hong Kong under Grant 9380034.

L. Zhou, V. Jandhyala, and Q. Li are with the Department of Electrical Engineering, University of Washington, Seattle, WA 98195 USA.

L. Tsang is with the Department of Electrical Engineering, University of Washington, Seattle, WA 98195 USA, and also with the Department of Electronic Engineering, City University of Hong Kong, Kowloon, Hong Kong.

C. H. Chan is with the Department of Electronic Engineering, City University of Hong Kong, Kowloon, Hong Kong.

Digital Object Identifier 10.1109/TGRS.2004.830639

with the second-order SPM method, which give the same results as the small slope approximation method for emissivity [19], [20]. It was found that the second-order SPM method gives poor results for cases when the rms slope is large. But the use of Gaussian correlation function is not appropriate for soil surfaces because the computed backscattering coefficients are many decibels below that of measurements. The exponential correlation function is a more realistic choice for soil surface, and it has been shown that exponential correlation function can be used to match active remote sensing experimental data. Surfaces with exponential correlation function have scale features that are finer and more irregular than that of a Gaussian correlation function of the same rms height and correlation length. On the other hand, the use of pulse basis functions is not able to provide accurate results of emissivity for the exponential correlation functions although they provide adequate results in decibel scale for backscattering coefficients [12]. For the exponential correlation functions, we have used pulse basis functions with many points per wavelength and using a high order of integration quadrature to calculate the impedance matrix elements. However, there was no convergence in emissivity. The energy conservation was also poor. Recent emphases on microwave remote sensing of soil moisture are moving toward a combination of active and passive remote sensing measurements, e.g., HYDROS satellite mission. Thus, it is important to have the same characterization, i.e., exponential correlation functions, in both active and passive remote sensing.

In this paper, we treat random rough surfaces as Gaussian random processes with non-Gaussian correlation functions. By using Rao–Wilton–Glisson (RWG) basis functions, we show that the accuracy of emissivities calculations is improved significantly for the case of exponential correlation functions. We implemented the SMCG method with the RWG basis functions [21] by projecting the triangular elements into the canonical grid. In the past, the Stratton–Chu formulation was used for the pulse basis functions. To implement the RWG basis functions, we use the Poggio–Miller–Chang–Harrington–Wu (PMCHW) formulation [22]. We present results of emissivities of soil surfaces with exponential correlation functions and ocean surfaces with ocean spectrum. Energy conservation checks are provided. These are essential because emissivity is calculated by the formula emissivity = transmissivity = 1 minus scattering. However, if the energy conservation check is such that transmissivity plus scattering is not equal to unity, then there is an ambiguity whether emissivity should be equal to transmissivity or equal to one minus scattering. This has been the difficulty with the classical Kirchoff approximation, which does not obey energy conservation. We compare the numerical results between SMCG/Pulse and SMCG/RWG. The numerical results of emissivities of soils are presented at both L- and C-bands and at multiple incidence angles for the same physical roughness parameters. We also present the brightness temperatures for ocean surfaces with various wind speeds. The numerical results are compared with those from the second-order small perturbation method (SPM) [23], [24]. Comparisons are also made with experimental emissivity measurements of soil surfaces. Parallel computations have been implemented in this work.

II. GENERAL FORMULATION

Consider a tapered plane wave [17] $\vec{E}^{\text{inc}}(\vec{r})$ and $\vec{H}^{\text{inc}}(\vec{r})$, with a time dependence of $e^{-i\omega t}$, impinging upon a two-dimensional (2-D) dielectric rough surface with a random height profile $z = f(x, y)$. Incident electric and magnetic fields $\vec{E}^{\text{inc}}(\vec{r})$ and $\vec{H}^{\text{inc}}(\vec{r})$ create equivalent electric and magnetic surface currents $\vec{J}(r)$ and $\vec{M}(r)$ on the rough surface. In the following, $\epsilon_{1,2}$ and $\mu_{1,2}$ represent the permittivity and the permeability, respectively, of the upper and lower half-spaces. Also, $k_{1,2} = \omega(\epsilon_{1,2}\mu_{1,2})^{1/2}$, and $\eta_{1,2} = (\mu_{1,2}/\epsilon_{1,2})^{1/2}$. To implement the RWG basis functions, we use the PMCHW formulation, which is summarized below. To obtain \vec{J} and \vec{M} , the PMCHW formulation enforces the continuity of the tangential electric- and magnetic-field components on the surface S

$$\begin{aligned} \vec{E}^{\text{inc}}(\vec{r})|_{\text{tan}} &= (L_1 + L_2)\vec{J}(\vec{r})|_{\text{tan}} - (K_1 + K_2)\vec{M}(\vec{r})|_{\text{tan}} \end{aligned} \quad (1)$$

$$\begin{aligned} \vec{H}^{\text{inc}}(\vec{r})|_{\text{tan}} &= (K_1 + K_2)\vec{J}(\vec{r})|_{\text{tan}} + \left(\frac{1}{\eta_1^2}L_1 + \frac{1}{\eta_2^2}L_2\right)\vec{M}(\vec{r})|_{\text{tan}} \end{aligned} \quad (2)$$

where the operators $L_{1,2}$ and $K_{1,2}$ are defined by

$$\begin{aligned} L_{1,2}\vec{X}(\vec{r}) &= \int_S ds' \left[-i\omega\mu_{1,2}\vec{X}(\vec{r}') + \frac{-i}{\omega\epsilon_{1,2}}\nabla\nabla' \cdot \vec{X}(\vec{r}') \right] \\ &\quad \cdot g_{1,2}(\vec{r}, \vec{r}') \end{aligned} \quad (3)$$

$$K_{1,2}\vec{X}(\vec{r}) = \int_S ds' \vec{X}(\vec{r}') \times \nabla g_{1,2}(\vec{r}, \vec{r}') \quad (4)$$

and $g_{1,2}(\vec{r}, \vec{r}')$ is the scalar Green's function in region 1 (air) and region 2 (lossy dielectric medium).

A. Emissivity and Brightness Temperature

The solution of the PMCHW yields the electric and magnetic surface current densities $\vec{J}(\vec{r})$ and $\vec{M}(\vec{r})$. These current densities can be used to evaluate the scattering field required in the computation of the bistatic scattering coefficient. The normalized bistatic scattering coefficient defined by

$$\gamma_{\beta\alpha}(\theta_s, \phi_s; \theta_i, \phi_i) = \frac{|S_{\beta}(\hat{k}_s)|^2}{2\eta_1 P_{\alpha}^{\text{inc}}}. \quad (5)$$

where α and β indicate the polarization of the incident and scattered waves, respectively, P_{α}^{inc} is the incident power, and the vertical and horizontal polarized scattered components are respectively

$$S_v(\hat{k}_s) = \frac{ik_1}{4\pi} \int_S ds [\hat{v}_s \cdot \eta_1 \vec{J} + \hat{h}_s \cdot \vec{M}] \exp(-ik_1 \hat{k}_s \cdot \vec{r}') \quad (6)$$

$$S_h(\hat{k}_s) = \frac{ik_1}{4\pi} \int_S ds [\hat{h}_s \cdot \eta_1 \vec{J} - \hat{v}_s \cdot \vec{M}] \exp(-ik_1 \hat{k}_s \cdot \vec{r}') \quad (7)$$

with $\hat{k}_s = \sin\theta_s \cos\phi_s \hat{x} + \sin\theta_s \sin\phi_s \hat{y} + \cos\theta_s \hat{z}$, $\hat{h}_s = -\sin\phi_s \hat{x} + \cos\phi_s \hat{y}$, and $\hat{v}_s = \cos\theta_s \cos\phi_s \hat{x} + \cos\theta_s \sin\phi_s \hat{y} - \sin\theta_s \hat{z}$. For scattering by a dielectric surface, the emissivity of

the rough surface at incident angle (θ_i, ϕ_i) is equal to transmissivity. By reciprocity and energy conservation, it is equal to

$$e_\beta(\theta_i, \phi_i) = 1 - \frac{1}{4\pi} \int \int [\gamma_{\beta h}(\theta_s, \phi_s; \theta_i, \phi_i) + \gamma_{\beta v}(\theta_s, \phi_s; \theta_i, \phi_i)] \sin \theta_s d\theta_s d\phi_s. \quad (8)$$

In this paper, we use (8) to calculate emissivity. In passive remote sensing, the brightness temperature T_B of the medium is measured at the observation angle (θ_i, ϕ_i) . The brightness temperature is $T_B(\theta_i, \phi_i) = e_\beta(\theta_i, \phi_i)T$ where T is the physical temperature of the medium in degrees kelvin.

B. Energy Conservation Verification

Energy conservation check is essential because emissivity as calculated in (8) is based on energy conservation. If the energy conservation check is such that transmissivity + scattering is not equal to unity, then there is an ambiguity whether emissivity should be equal to transmissivity or equal to one minus scattering. For a penetrable medium, absorptivity $a(\theta_i)$ is equal to transmissivity. The absorptivity and reflectivity $r(\theta_i)$ can be calculated in term of the surface fields

$$a(\theta_i) = \frac{P_a}{P_{\text{inc}}} = \frac{\int_S ds \hat{n} \cdot \frac{1}{2} \text{Re}[\overline{E} \times \overline{H}]}{P_{\text{inc}}} \quad (9)$$

$$r(\theta_i) = \frac{P_s}{P_{\text{inc}}} = \frac{\int_S ds \hat{n} \cdot \frac{1}{2} \text{Re}[\overline{E}_s \times \overline{H}_s]}{P_{\text{inc}}} \quad (10)$$

where \overline{E} and \overline{H} are the total electrical and magnetic surface fields, respectively, while \overline{E}_s and \overline{H}_s are the surface scattered fields. They are calculated as $\overline{E}_s = \overline{E} - \hat{n} \times \overline{E}^{\text{inc}} = -\overline{M} - \hat{n} \times \overline{E}^{\text{inc}}$, and $\overline{H}_s = \overline{H} - \hat{n} \times \overline{H}^{\text{inc}} = \overline{J} - \hat{n} \times \overline{H}^{\text{inc}}$. The surface fields are calculated for each realization, and we can calculate absorptivity and reflectivity using (9) and (10), respectively.

Then, we check whether $a(\theta_i) + r(\theta_i)$ is equal to unity. In this paper, results of $a(\theta_i) + r(\theta_i)$ are provided for the simulations.

III. NUMERICAL METHOD OF SMCG/RWG

To solve the PMCHW equation, the Galerkin's procedure is used to obtain the impedance matrix. The RWG basis is chosen for both expansion and weighting function. The definition of the RWG basis function associated with the n th interior edge is given by [21]

$$\Lambda_n(\vec{r}) = \begin{cases} \frac{l}{2S_n^+} \rho_n^+, & \vec{r} \in S_n^+ \\ \frac{l}{2S_n^-} \rho_n^-, & \vec{r} \in S_n^- \end{cases} \quad (11)$$

where S_n^\pm is the area of the two triangular patches, respectively, and l is the length of the interior edge. The surface current unknown $\overline{J}(\vec{r})$ and $\overline{M}(\vec{r})$ are represented in terms of linear combination of a set of basis functions. The surface current is tangential at the exterior edges, and there is no current across the exterior edges. The current normal to the interior edge is continuous. The RWG basis is a more accurate way than pulse basis function to model the shape of surfaces and to represent the surface currents.

Applying the RWG basis to (1) and (2) produces the matrix equation

$$[Z]I = V. \quad (12)$$

In the SMCG method, the matrix equation (1) and (2) is solved in an iterative manner (e.g., conjugate gradient method). The impedance matrix is decomposed into the sum of a sparse matrix $[Z^s]$, denoting the strong near interactions, and a dense matrix $[Z^w]$, denoting the weak far interactions. The two integrals of interest in the full-wave case are

$$I_A = \int_T dr' \frac{\exp(ik|\vec{r} - \vec{r}'|)}{|\vec{r} - \vec{r}'|} \quad (13)$$

$$\overline{I}_B(m) = \int_T dr' \frac{\exp(ik|\vec{r} - \vec{r}'|)}{|\vec{r} - \vec{r}'|} \vec{\rho}'_m, \quad m = 1, 2, 3. \quad (14)$$

For the near-field interactions, we take the numerical integration over both the expansion and weighting functions, using numerical quadrature rule. In such a case, the integral is approximated by a weighted sum, with n_{int} terms

$$I_{ji} \approx A_i \sum_{k=1}^{n_{\text{int}}} \frac{w_k}{|\vec{r}_j - \vec{r}_k'|} \quad (15)$$

where \vec{r}_j is the point in the observation triangle T_j , and \vec{r}_k' is the source point in the area-barycentric-triangular coordinate system (α, β, γ) , which is equal to $\alpha\vec{r}_1 + \beta\vec{r}_2 + \gamma\vec{r}_3$. The \vec{r}_1 , \vec{r}_2 , and \vec{r}_3 represent the vertices of the source triangle T_i , and A_i is the area of T_i .

Let $|\vec{r} - \vec{r}'| = R$. It is clear that when R is close to 0, the above integrals are singular and hence cannot be integrated numerically using the quadrature rule. When the integral is evaluated for the self term ($i = j$), the unbounded nature of the Green's functions necessitates an analytic approach finding the integral [25]. The following are integrals that are evaluated analytically:

$$\int_T \frac{dS'}{R} = \sum_{i=1}^3 \widehat{P}_i^0 \cdot \widehat{u}_i \left[P_i^0 \ln \frac{R_i^+ + l_i^+}{R_i^- + l_i^-} - |d| \cdot \left(\tan^{-1} \frac{P_i^0 l_i^+}{(R_i^0)^2 + |d| R_i^+} - \tan^{-1} \frac{P_i^0 l_i^-}{(R_i^0)^2 + |d| R_i^-} \right) \right] \quad (16)$$

$$\int_T (\vec{\rho}' - \vec{\rho}) \frac{dS'}{R} = \frac{1}{2} \sum_{i=1}^3 \widehat{u}_i \left[(R_i^0)^2 \ln \frac{R_i^+ + l_i^+}{R_i^- + l_i^-} + R_i^+ l_i^+ - R_i^- l_i^- \right] \quad (17)$$

where $\vec{\rho}'$ is the location of a point in the triangle with respect to a global coordinate system, and $\vec{\rho}$ is the projection of the test point into the plane of the triangle. The vector $\vec{\rho}' - \vec{\rho}$, thus, points from a point in the triangle to the projection of the test point onto the plane of the triangle. Integral (13) can be divided into two integrals, one which can be integrated using (16), and one which

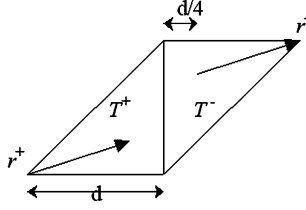


Fig. 1. RWG basis function.

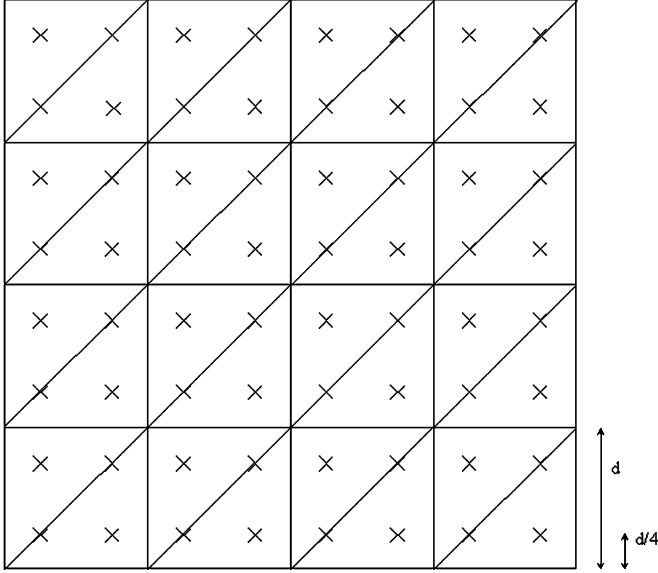


Fig. 2. Projection of rough surface on the X-Y plane and canonical grid depicted by cross points.

has no singularity. Numerical quadrature rules can be applied to the one without singularity.

$$\int_T dr' \frac{\exp(ikR)}{R} = \int_T dr' \frac{1}{R} + \int_T dr' \frac{\exp(ikR) - 1}{R}. \quad (18)$$

Integral (17) can also be rewritten in a form such that a combination of analytic and numerical integration can be used

$$\int_T dS' (\vec{p}'_m) \frac{\exp(ikR)}{R} = \int_T dS' (\vec{p}' - \vec{p}) \frac{\exp(ikR)}{R} + (\vec{p}' - \vec{p}_m) \int_T dS' \frac{\exp(ikR)}{R} \quad (19)$$

where the vector \vec{p}_m is the position vector of vertex m ($m = 1, 2, 3$) of triangle T in a global system. Note that, as required by patch-by-patch filling of the method-of-moments (MoM) matrix elements, none of the integrals are dependent on the vertex m nor the local edge number. The dependence on m arises only as vectors outside the integrals.

For the far-field interactions, the Green's functions are smooth over the integration domains of the impedance matrix elements integrals. We then only use the one-point approximation. We choose a point $(1/4, 1/4)$ in the triangle instead of the centroid $(1/3, 1/3)$, as depicted in Fig. 1. Thus, the points at $(1/4, 1/4)$ of triangles fall in the canonical grid, as shown in Fig. 2 by cross points. By using this judicious procedure, we only need to make Taylor expansion vertically and not horizontally

TABLE I
EMISSIVITY WITH VARIOUS REALIZATION, FOR HORIZONTAL POLARIZATION AT THE INCIDENT ANGLE OF 30° WITH SOIL ROUGH SURFACE rms HEIGHT 0.40 cm, CORRELATION LENGTH 8.4 cm, IN C-BAND

Various Realization	Absorptivity	Scattering	1-Scattering (Emissivity)	Energy Cons. Check
1	0.61800	0.38880	0.61120	1.0068
2	0.61542	0.39253	0.60747	1.0079
3	0.61537	0.39211	0.60789	1.0075
4	0.61585	0.38977	0.61023	1.0056
Average	0.61616	0.39080	0.60920	1.0059

to translate to the canonical grid in the SMCG implementation [17]. Efficient evaluation of the far-interaction contributions in the matrix-vector multiplication is reduced to a convolution between the Green's function and the current vector. We choose r_d as the neighborhood distance (e.g., $r_d = 2\lambda$). Let $\rho_R = \sqrt{(x-x')^2 + (y-y')^2}$ be the horizontal separation between two points on the rough surface $(x, y, f(x, y))$ and $(x', y', f(x', y'))$. Since the weak matrix elements satisfy the condition $\rho_R > r_d \gg |f(x, y) - f(x', y')|$, we can expand the Green's function in a Taylor's series about the flat surface using z_d^2/ρ_R^2 as the small parameter where $z_d = f(x, y) - f(x', y')$. Due to the translational invariant kernels in the Green's functions, the weak-matrix vector multiplication can be efficiently performed via 2-D FFT. In this work, we use six terms of the expansion series.

IV. NUMERICAL RESULTS AND DISCUSSION

In this section, we illustrate the numerical simulation results of three types of random rough surfaces. They are Gaussian rough surfaces with Gaussian correlation function, exponential correlation function and ocean spectrum. The surface area is 8×8 square wavelengths. Rough surfaces modeled with as many as 96 266 current basis functions are solved. All numerical results are computed using parallel computation with the near interaction distance 2.1λ . We use $T = 283$ K as the physical temperature. We tabulate the results of emissivities so that the accuracies can be ascertained and readers will find it easier to make future comparisons. Energy conservation checks are given by adding $a(\theta_i)$ and $r(\theta_i)$.

We have gained extensive experience in our course of numerical simulations. On the one hand, that passive remote sensing requires great accuracy in energy conservation that is not required in active remote sensing. On the other hand, passive remote sensing can be easier than active remote sensing in other aspects. For example, in active remote sensing, the results fluctuate from realization to realization because of speckle. However, in passive remote sensing, the emissivity requires an integration of bistatic scattering cross sections over 2π solid angles. The integration smooths out the speckle fluctuations that exist in the bistatic coefficients. Our experience indicates that passive remote sensing needs a lot fewer realizations than active remote sensing. We present one example in Table I to show the values with various realizations.

In the past, extensive studies have also been done with varying sample size from 8 wavelength \times 8 wavelengths, to 16 wavelengths \times 16 wavelengths, etc. The physical meaning is that the

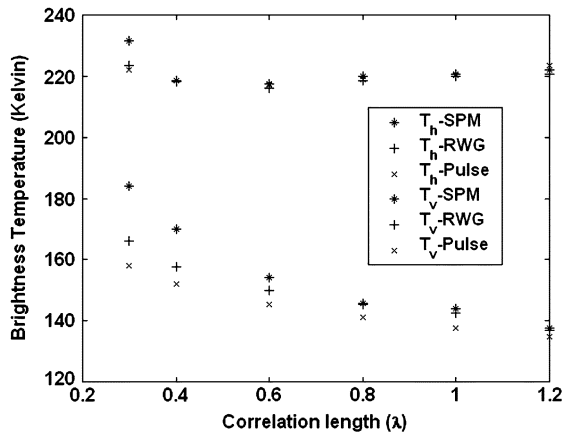


Fig. 3. Brightness temperature of Monte Carlo simulations averaged over five realizations as a function of correlation lengths and comparisons with those from the second-order small perturbation method, and from the PBTG/Pulse. The case is with rms height of 0.1 wavelength, relative permittivity of $17 + 2i$, and physical temperature of 283 K at observation angle of 50° .

coherent interaction of waves are limited in extent. Thus, if coherent interaction is limited to 8×8 square wavelengths, then incoherent superpositions can be exercised beyond 8×8 wavelengths. Numerical solutions of Maxwell equations need to be done for an area 8×8 square wavelengths. The surface area is $8 \text{ wavelengths} \times 8 \text{ wavelengths}$ in this paper. The surface length of eight wavelengths is much larger than the correlation lengths.

A. Emissivities and Bistatic Scattering Cross Sections of Gaussian Surfaces With Gaussian Correlation Function

We compare the brightness temperature results of rough surfaces with Gaussian correlation function using three methods: SMCG with pulse basis functions, SMCG with RWG basis functions and SPM. By SPM, we mean the common second-order SPM result of emissivity which is computing the coherent field to second order and incoherent field to first order [24]. In Fig. 3, the brightness temperatures are shown as functions of correlation length from 0.3 wavelength to 1.2 wavelength with a fixed value of rms height at 0.1 wavelength, for both transverse electric (TE) and transverse magnetic (TM) waves. The observation angle is 50° , and the relative permittivity is $17 + i2.0$. It is shown that the results of the three approaches agree very well for the case of TM wave incidence with one exception. The exception of the TM case is the deviation from the numerical solutions by SPM at the correlation length of 0.3 wavelength. In the case of TE wave incidence on rough surface with large rms slope, SMCG/Pulse gives lower results than SMCG/RWG by about 5 K. SPM gives good comparison for small slopes and becomes inaccurate by as much as 20 K for large slopes.

In Fig. 4, the bistatic scattering coefficients of the same surfaces are compared between the SMCG/RWG and SMCG/Pulse for the TE wave incidence at the incident angle of 50° . The rms height and correlation length of Gaussian surface are 0.1 and 1.0 wavelengths, and the relative permittivity is $17 + 2i$. The results are for a single realization. The comparison in Fig. 4 shows good agreement between two approaches. This shows that pulse basis functions can give accurate results for bistatic scattering coefficients but less accurate results for passive remote sensing. We plot the profiles of surface with exponential

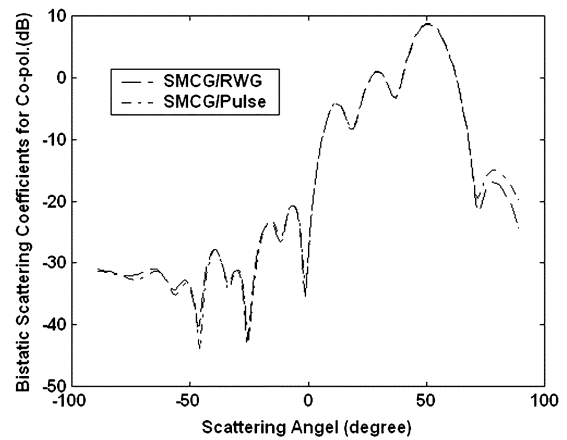


Fig. 4. Comparison of the bistatic scattering coefficients between the SMCG/RWG and the SMCG/Pulse for the TE wave incidence of copolarization. The case is with rms height of 0.1 wavelength, correlation length of 1.0 wavelength, and relative permittivity of $17 + 2i$ at observation angle of 50° .

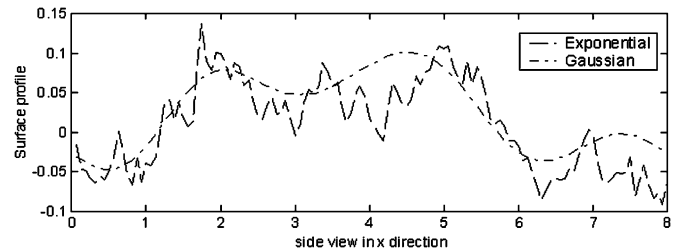


Fig. 5. Profiles of surface side views by exponential and Gaussian correlation functions.

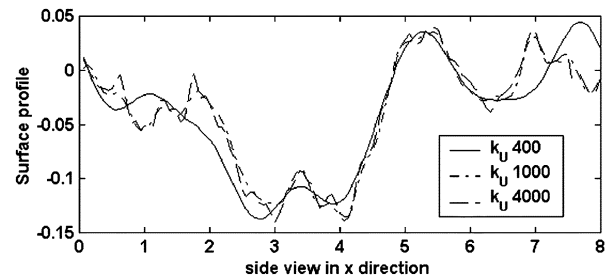


Fig. 6. Profiles of surface side views by ocean spectrum with various values of up-limit k_U .

correlation function, Gaussian correlation function, and ocean spectrum shown in Figs. 5 and 6. Fig. 5 shows the fine irregular features that exist in exponential correlation function. This is the cause of the large emissivity differences between Gaussian correlation function and exponential correlation function. Fig. 6 shows that new features of irregularity in the roughness profiles when the upper limit of ocean spectrum is increased. It is apparent that surfaces with exponential correlation function and ocean spectrum can have fine-scale features with large rms slope. Although Gaussian correlation function is inappropriate for soil surface, the characterization of soil surface remains an important problem. Exponential correlation function is just a popular and better choice than Gaussian correlation function. It is to be noted that exponential correlation function does not have rms slopes if the roughness spectrum upper limit is set at infinity. However, in actual implementation in this paper, 16 points per

TABLE II
THE MEASURED SURFACE ROUGHNESS PARAMETERS AND THE
RELATIVE PERMITTIVITIES OF WET SOIL

	rms height (cm)	Correlation length(cm)	Relative permittivity	
			1.5 GHz	4.75 GHz
Field I	0.4	8.4	15.57+i3.71	15.42+i2.15
Field 3	1.12	8.4	15.34+i3.66	15.23+i2.12

TABLE III
EMISSIVITY OF SOIL SURFACES WITH rms HEIGHT 0.40 cm,
CORRELATION LENGTH 8.4 cm, IN L-BAND

Polar.	Inc. angle	Emissivity	Energy cons.	Emiss.of flat	$\Delta Emiss.$ (rough-flat)	Emissivity by SPM
TE	30	0.5891	1.0065	0.5851	0.0040	0.6007
TE	40	0.5465	0.9936	0.5413	0.0052	0.5560
TE	50	0.4930	0.9926	0.4806	0.0124	0.4950
TM	30	0.6951	1.0048	0.6893	0.0058	0.7036
TM	40	0.7397	1.0040	0.7342	0.0055	0.7476
TM	50	0.7997	1.0061	0.7969	0.0028	0.8084

TABLE IV
EMISSIVITY OF SOIL SURFACES WITH rms HEIGHT 0.40 cm,
CORRELATION LENGTH 8.4 cm, IN C-BAND

Polar.	Inc. angle	Emissivity	Energy cons.	Emiss.of flat	$\Delta Emiss.$ (rough-flat)	Emissivity by SPM
TE	30	0.6092	1.0060	0.5923	0.0217	0.6214
TE	40	0.5752	0.9942	0.5485	0.0267	0.5888
TE	50	0.5136	0.9936	0.4875	0.0261	0.5288
TM	30	0.7219	0.9932	0.6964	0.0255	0.7302
TM	40	0.7563	1.0034	0.7411	0.0152	0.7728
TM	50	0.8086	1.0018	0.8035	0.0051	0.8290

wavelength is used to generate the roughness profile. This corresponds to setting an upper limit on the roughness spectrum.

B. Soil Surfaces

The ground truth measurements are from Oh *et al.* [26]. The physical surface parameters, based on exponential correlation function, are the same for both L- and C-bands. Field I is smooth and Field III is rough. The measured rough-surface parameters and relative permittivities of wet soil are listed in Table II. The upper limits of wavenumber in the spectrum are 3.55 and 11.24 cm, respectively, at L- and C-bands. The numerical results are presented with various incident angle and compared with those from SPM.

In Tables III and IV, we tabulate the emissivity results in L- and C-bands, respectively, for the smooth field I with rms height of 0.4 cm and correlation length of 8.4 cm. It is shown that surface roughness increases the brightness temperature over flat surfaces for both horizontal and vertical polarizations. The difference of emissivity between rough surface and flat surface is larger in C-band than in L-band. In this case, the results from SPM are in agreement with NMM3D.

Field III has larger slope with rms height of 1.12 cm and correlation length of 8.4 cm. The results are listed in Tables V and VI, for L- and C-bands, respectively. In this case, the SPM results do not agree with NMM3D.

We also present numerical emissivities of soil at horizontal polarization with large incidence angle at 55° for the cases with surface rms heights of 0.05λ to 0.15λ , and correlation lengths of 0.4λ to 0.8λ . The energy conservation is within 2% (that is,

TABLE V
EMISSIVITY OF SOIL SURFACES WITH rms HEIGHT 1.12 cm,
CORRELATION LENGTH 8.4 cm, IN L-BAND

Polar.	Inc. angle	Emissivity	Energy cons.	Emiss.of flat	$\Delta Emiss.$ (rough-flat)	Emissivity by SPM
TE	30	0.6351	1.0031	0.5877	0.0474	0.6920
TE	40	0.5944	0.9970	0.5439	0.0505	0.6482
TE	50	0.5338	0.9968	0.4831	0.0507	0.5838
TM	30	0.7380	1.0023	0.6919	0.0461	0.7840
TM	40	0.7658	1.0045	0.7367	0.0291	0.8194
TM	50	0.8140	1.0015	0.7992	0.0148	0.8671

TABLE VI
EMISSIVITY OF SOIL SURFACES WITH rms HEIGHT 1.12 cm,
CORRELATION LENGTH 8.4 cm, IN C-BAND

Polar.	Inc. angle	Emissivity	Energy cons.	Emiss.of flat	$\Delta Emiss.$ (rough-flat)	Emissivity by SPM
TE	30	0.7388	1.0045	0.5947	0.1441	0.9385
TE	40	0.7028	1.0062	0.5508	0.1520	0.9052
TE	50	0.6535	1.0082	0.4898	0.1637	0.8466
TM	30	0.7962	0.9912	0.6988	0.0974	0.9901
TM	40	0.8058	0.9900	0.7434	0.0624	1.0020
TM	50	0.8318	0.9869	0.8056	0.0262	1.0080

TABLE VII
NUMERICAL RESULTS FOR SOIL SURFACES WITH SOIL MOISTURE 30%,
PERMITTIVITY OF $31.5 + i4.11$, HORIZONTAL POLARIZATION AT ANGLE = 55°

rms height (λ)	Corr. length (λ)	Emissivity	Energy cons.	$\Delta Emiss.$ (rough-flat)
0.15	0.4	0.57063	1.0108	0.23301
0.15	0.6	0.52695	1.0127	0.18933
0.15	0.8	0.49767	1.0108	0.16005
0.10	0.4	0.45459	1.0096	0.11697
0.10	0.6	0.42733	1.0081	0.08971
0.10	0.8	0.41414	1.0070	0.07652
0.05	0.4	0.36086	1.0096	0.02324
0.05	0.6	0.35304	1.0082	0.01542
0.05	0.8	0.34774	1.0076	0.01012

TABLE VIII
NUMERICAL RESULTS FOR SOIL SURFACES WITH SOIL MOISTURE 20%,
PERMITTIVITY OF $17.7 + i2.26$, HORIZONTAL POLARIZATION AT ANGLE = 55°

rms height (λ)	Corr. length (λ)	Emissivity	Energy cons.	$\Delta Emiss.$ (rough-flat)
0.10	0.4	0.55027	1.020	0.12385
0.10	0.6	0.52250	1.017	0.09608
0.10	0.8	0.50363	1.016	0.07721
0.05	0.4	0.45223	1.013	0.02581
0.05	0.6	0.44322	1.011	0.01680
0.05	0.8	0.43759	1.010	0.01117

less than 1.02 or more than 0.98). Table VII is for soil moistures of 30% with the permittivity of $31.5 + i4.11$, while Table VIII is for soil moisture of 20% with the permittivity of $17.7 + i2.26$.

1) *Comparison With Experimental Data:* Numerical results are compared with brightness temperature measurements of soil surfaces [27]. The measurements were conducted at Texas A&M University [28], [29] for 16 profiles of soil moisture and temperatures. The brightness temperatures were measured at nadir incidence of $\lambda = 21$ cm. Ground truth measurements of soil moisture and temperature were taken at several depths down to 15 cm. The standard deviation of height σ was also measured and was 2.6 cm. The permittivities are calculated by

TABLE IX
COMPARISON OF NUMERICAL RESULTS (NMM) WITH EXPERIMENTAL BRIGHTNESS
TEMPERATURE MEASUREMENTS. SURFACE rms HEIGHT $\sigma = 2.6$ cm

Data Set	correlation length (cm)	Relative permittivity	Physical temp.(K)	Flat $T_B(K)$	NMM $T_B(K)$	Experiment
CM 3	7.0	29.4 + <i>i</i> 3.86	296.0	160.45	217.0	216.8
CM 4	8.2	20.05 + <i>i</i> 2.57	295.7	190.56	227.4	224.2
CM 8	7.6	23.57 + <i>i</i> 3.05	303.7	177.68	223.6	221.1
CM 9	13.0	15.98 + <i>i</i> 2.03	297.8	212.91	227.4	223.53

using the mixing formula at a wavelength of 21 cm [30], based on soil moisture measurements in each layer. Then, they are averaged from the soil depth of 0–2 cm. The weighted physical temperature, based on measurements, was used for each profile. Since there was no measurement of the horizontal correlation length, the correlation length within a reasonable range was chosen to match the data. In Table IX we list the results for four of the 16 profiles. These four cases are with large permittivities.

In performing numerical simulations, the exponential correlation function with upper wavenumber limit of 3.38/cm is employed to generate rough surfaces. The correlation lengths l are the same as used in [27]. As shown in Table IX, the numerical results are in agreement with the experiments. The differences between the numerical simulations and the experiments are no more than 3 K. Since the brightness temperatures of rough surfaces with high permittivities can be more than 40 K different from that of smooth surfaces, the difference of 3 K between numerical results and measurements is acceptable.

C. Ocean Surfaces

To describe the wind-induced ocean surfaces, we use the semiempirical Durden–Vesecky spectrum [31]–[34]. In the model, a_0 is the absolute magnitude of the spectrum. Since a parametric analysis has been carried out showing that $a_0 = 0.008$ gives the best agreement with experiment data in [32], a_0 of 0.008 is used for calculations in this paper. The wavenumber cutoff k_L and k_U are the key parameters in the spectrum, corresponding to the low-frequency limit and the high-frequency limit of ocean spectrum, respectively. The quantities k_L and k_U can be selected to control the rms height and fine-scale structures [32]. The physical temperature is 283 K. The permittivities of the sea water at 19 GHz is $28.9541 + i36.8340$.

For the sake of illustration, we show the results for the hypothetical situations of wind speed 10 and 20 m/s. It is to be noted that 20 m/s is closer to gale force winds under hurricane conditions. With such high winds, the ocean surface tends to have white capping and may not be simply represented by an ocean spectrum. In Fig. 6, the ocean surface profiles are generated at the wind speed of 20 m/s with various k_U , while k_L is equal to 100 rad/m. For larger value of k_U , there are more fine-scale structures. The roughness parameter $k\sigma$ for these three cases were 0.4263, 0.4415, and 0.4715 (i.e., rms height σ : 0.1071, 0.1110, and 0.1185 cm), respectively. Note that by bandlimiting the ocean spectrum, the rms heights are small, and there are substantial differences of these three cases. The corresponding results of emissivities and brightness temperature at the incident angle of 50° are listed in Table X. In Table X, k_U is chosen to

TABLE X
EMISSIVITY AND BRIGHTNESS TEMPERATURE WITH VARIOUS
VALUES OF k_U . $k_L = 100$ rad/m

Polar.	k_U (rads/m)	Emissivity	Energy cons.	Emiss.of flat	$T_B(K)$	ΔT_B (rough - flat)
TE	400	0.3118	0.9921	0.2872	88.2	6.96
TE	1000	0.3207	0.9920	0.2872	90.8	9.48
TE	4000	0.3233	0.9915	0.2872	91.5	10.22
TM	400	0.5477	0.9967	0.5594	155.0	-3.31
TM	1000	0.5550	0.9961	0.5594	157.1	-1.25
TM	4000	0.5604	0.9925	0.5594	158.6	0.30

TABLE XI
EMISSIVITY OF OCEAN SURFACES AT WIND SPEED 10 m/s WITH
 $k_L = 100$ rad/m AND $k_U = 4000$ rad/m

Polar.	Inc. angle	Emissivity	Energy cons.	Emiss. of flat	ΔT_B (rough - flat)
TE	30	0.3723	1.0028	0.3662	1.72
TE	40	0.3427	0.9956	0.3319	3.06
TE	50	0.3056	0.9927	0.2872	5.21
TM	30	0.4744	0.9960	0.4555	5.35
TM	40	0.4991	1.0040	0.4971	0.57
TM	50	0.5534	0.9966	0.5594	-1.70

TABLE XII
EMISSIVITY OF OCEAN SURFACES AT WIND SPEED 20 m/s WITH
 $k_L = 100$ rad/m AND $k_U = 4000$ rad/m

Polar.	Inc. angle	Emissivity	Energy cons.	Emiss. of flat	ΔT_B (rough - flat)
TE	30	0.3863	1.0006	0.3662	5.69
TE	40	0.3584	0.9986	0.3319	7.5
TE	50	0.3233	0.9915	0.2872	10.2
TM	30	0.4898	0.9980	0.4555	9.7
TM	40	0.5015	0.9971	0.4971	1.25
TM	50	0.5604	0.9925	0.5594	0.30

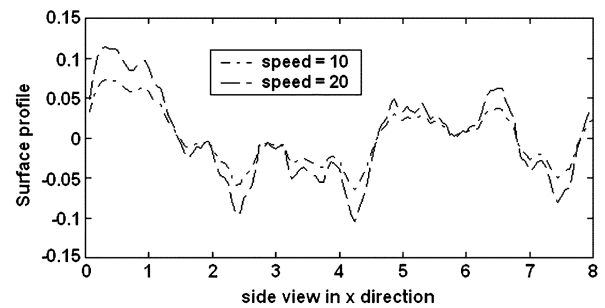


Fig. 7. Profiles of surface side views for various wind speeds, with $k_L = 100$ rad/m and $k_U = 4000$ rad/m.

be 400, 1000, and 4000 rad/m with fixed $k_L = 100$ rad/m. It is shown that the difference of brightness temperature between rough surface and flat surface increases with the increase of k_U . The differences can be attributed to the fine-scale features and

TABLE XIII
CPU TIME (SECONDS) AND MEMORY (MEGABYTES)

Number of unknowns	Memory (MB)	Mtx ele.stored for near field	Near field (sec/iteration)	Far field (sec/iteration)	Total time(sec)
23562	1495.5	3.2×10^6	39.3	5.8	848.2
96266	14543.8	51.3×10^6	637.9	21.0	3930.6

the differences in rms heights for these three cases. Table XI is for the case at wind speed 10 m/s with corresponding $k\sigma$ equal to 0.3156 (i.e., rms height σ : 0.079 cm). k_L equal to 100 rad/m, and k_U is 4000 rad/m. For the case at the wind speed of 20 m/s with $k\sigma$ equal to 0.4715, the brightness temperatures are listed in Table XII. The profiles of sea surfaces at the wind speeds of 10 and 20 m/s are plotted in Fig. 7 for reference, while k_U is equal to 4000 rad/m.

V. CPU AND MEMORY REQUIREMENT

Numerical results are computed using parallel computation provided by the Beowulf cluster at the Wireless Communication Research Center of the City University of Hong Kong consisting of 32 processors in 16 personal computers with dual Pentium III 1.0-GHz CPUs and 2-GB RAM for each computer. We tabulate CPU and memory in Table XIII. The values are for the case of TE wave at 30° incidence on field I with rms height of 0.4 cm and correlation length of 8.4 cm. The CPU can be different from case to case depending on the surface roughness, permittivity, and incidence angle. Since both the CPU time and memory storage are large for the calculation of near-field interaction, the matrix elements of near-field interaction are computed once and stored among all processors. The surface current unknown is in term of an interior edge, which is associated with two patches of RWG basis function. For the case of 96 266 unknowns, the total consumed time in parallel code is 3930.6 s, in which it takes 637.9 s for calculation of near-field interactions and 21.0 s multiplied by the number of iteration for far-field interactions. The average number of iterations is 100. In this case, the combined memory usage among 32 processors is 14 543.8 MB.

VI. CONCLUSION

A numerical Maxwell model is developed for solving the problem of scattering by random rough surfaces to calculate emissivities for applications in passive microwave remote sensing of soil and ocean surfaces. To emphasize the new contribution with respect to the paper published in July 2000 [8], this present paper computes the emissivity of a Gaussian surface with an exponential correlation function, while the previous paper uses a Gaussian correlation function. The use of an exponential correlation function is important for a rough soil surface, as it is gaining wide acceptance in recent years that a Gaussian correlation function is not appropriate, while exponential function results compare favorably with experiments. However, surfaces with exponential correlation functions contain fine features with large slopes. To calculate emissivity accurately for such surfaces requires substantial changes of the MoM formulation from the previous paper. In this paper, the accuracies of emissivity calculations are improved by

using RWG basis functions. We further use a sparse matrix canonical method to solve the PMCHW integral equations by the MoM. The emissivities are calculated for surfaces with Gaussian correlation function, exponential correlation function, and ocean spectrum. The emissivities of soils are presented at both L- and C-bands and at multiincidence angles for the same physical roughness parameters. The brightness temperatures for ocean are illustrated for various wind speeds. The energy conservation tests for all the cases are given. Needless to say that analytic theory can give better results than numerical simulations when the roughness is very small. For example, if the difference is only 0.0001 between a rough surface and a flat surface, analytic theory will be superior because numerical simulations are hampered by numerical noise. But, in practice, for the case of soils, the important cases are when there are appreciable differences of emissivities between rough surface and flat surface. For small differences, practitioners will be happy to know that roughness effects only give small differences. From this point of view, numerical simulations have wider regimes of validity than analytic theory. Furthermore, with the continual development of the computational method, and the ever-increasing capabilities of computers, it is anticipated that both accuracies and CPU will continue to increase in numerical simulations giving better results for NMM3D.

REFERENCES

- [1] L. Tsang, J. A. Kong, and R. Shin, *Theory of Microwave Remote Sensing*. New York: Wiley, 1985.
- [2] A. Ishimaru, *Wave Propagation and Scattering in Random Media*. New York: Academic, 1978.
- [3] R. L. Wagner, J. Song, and W. C. Chew, "Monte Carlo simulation of electromagnetic scattering from two-dimensional random rough surface," *IEEE Trans. Antennas Propagat.*, vol. 45, pp. 235–245, Feb. 1997.
- [4] V. Jandhyala, B. Shanker, E. Michielssen, and W. C. Chew, "Fast algorithm for the analysis of scattering by dielectric rough surfaces," *J. Opt. Soc. Amer. A*, pp. 1877–1885, 1998.
- [5] K. Pak, L. Tsang, C. H. Chan, and J. Johnson, "Backscattering enhancement of vector electromagnetic waves from two-dimensional perfectly conducting random rough surfaces based on Monte Carlo simulations," *J. Opt. Soc. Amer. A*, vol. 12, no. 11, pp. 2491–2499, 1995.
- [6] K. Pak, L. Tsang, and J. Johnson, "Numerical simulations and backscattering enhancement of electromagnetic waves from two-dimensional dielectric random rough surfaces with the sparse-matrix canonical grid method," *J. Opt. Soc. Amer. A*, vol. 14, no. 7, pp. 1515–1529, July 1997.
- [7] Q. Li, L. Tsang, K. S. Pak, and C. H. Chan, "Bistatic scattering and emissivities of random rough dielectric lossy surfaces with the physics-based two-grid method in conjunction with the sparse-matrix canonical grid method," *IEEE Trans. Antennas Propagat.*, vol. 48, pp. 1–11, Jan. 2000.
- [8] Q. Li, L. Tsang, J. C. Shi, and C. H. Chan, "Application of physics-based two-grid method and sparse matrix canonical grid method for numerical simulations of emissivities of soils with rough surfaces," *IEEE Trans. Geosci. Remote Sensing*, vol. 38, pp. 1635–1643, July 2000.
- [9] J. C. West, "Integral equation formulation for iterative calculation of scattering from lossy rough surfaces," *IEEE Trans. Geosci. Remote Sensing*, vol. 38, pp. 1609–1615, July 2000.
- [10] J. V. Toporkov and G. S. Brown, "Numerical simulations of scattering from time-varying, randomly rough surfaces," *IEEE Trans. Geosci. Remote Sensing*, vol. 38, pp. 1616–1625, July 2000.

- [11] H. T. Chou and J. T. Johnson, "Formulation of forward-backward method using novel spectral acceleration for the modeling of scattering from impedance rough surfaces," *IEEE Trans. Geosci. Remote Sensing*, vol. 38, pp. 605–607, Jan. 2000.
- [12] Q. Li, L. Zhou, L. Tsang, and K. S. Chen, "Numerical study of frequency and polarimetric dependence of the emissivities and backscattering coefficients of soil based on three dimensional Monte-Carlo simulations of Maxwell's equations," in *Proc. IGARSS*, Toronto, ON, Canada, June 2002.
- [13] L. Zhou, L. Tsang, V. Jandyala, and C. Chen, "Studies on accuracy of numerical simulations of emission from rough ocean-like surfaces," *IEEE Trans. Geosci. Remote Sensing*, vol. 39, pp. 1757–1763, Aug. 2001.
- [14] S. Q. Li, C. H. Chan, L. Tsang, Q. Li, and L. Zhou, "Parallel implementation of the sparse matrix/canonical grid method for the analysis of two-dimensional random rough surface (three-dimensional scattering problem) on a Beowulf system," *IEEE Trans. Geosci. Remote Sensing*, vol. 38, pp. 1600–1608, July 2000.
- [15] S. Q. Li, C. H. Chan, L. Tsang, and L. Zhou, "Microwave emission of rough ocean surfaces with full spatial spectrum based on the multilevel expansion method," *IEEE Trans. Geosci. Remote Sensing*, vol. 40, pp. 574–582, Mar. 2002.
- [16] M. Y. Xia and C. H. Chan, "Parallel analysis of electromagnetic scattering from random rough surfaces," *Electron. Lett.*, vol. 39, no. 9, pp. 710–712, May, 1st 2003.
- [17] L. Tsang, J. A. Kong, K. H. Ding, and C. Ao, *Scattering of Electromagnetic Waves: Numerical Simulations*. New York: Wiley, 2001.
- [18] J. T. Johnson, R. Shin, L. Tsang, K. Pak, and J. A. Kong, "A numerical study of ocean polarimetric, polarimetric thermal emission," *IEEE Trans. Geosci. Remote Sensing*, vol. 37, pp. 8–20, Jan. 1999.
- [19] V. G. Irisov, "Small-slope expansion for thermal and reflected radiation from a rough surface," *Waves Random Media*, vol. 7, no. 1, pp. 1–10, Jan. 1997.
- [20] A. G. Voronovich, *Wave Scattering from Rough Surfaces*. New York: Springer-Verlag, 1994.
- [21] S. M. Rao, D. R. Wilton, and A. W. Glisson, "Electromagnetic scattering by surfaces of arbitrary shape," *IEEE Trans. Antennas Propagat.*, vol. 30, pp. 409–418, May 1982.
- [22] L. Medgyesi-Mitschang, J. Putnam, and M. Gedera, "Generalized method of moments for three-dimensional penetrable scatterers," *J. Opt. Soc. Amer. A*, vol. 12, pp. 1383–1398, 1994.
- [23] L. Tsang, J. A. Kong, and K. H. Ding, *Scattering of Electromagnetic Waves: Theories and Applications*. New York: Wiley, 2000.
- [24] L. Tsang and J. A. Kong, *Scattering of Electromagnetic Waves: Advanced Topics*. New York: Wiley, 2001.
- [25] D. R. Wilton, S. M. Rao, A. W. Glisson, D. H. Schaubert, O. M. Al-Bundak, and C. M. Butler, "Potential integrals for uniform and linear source distributions on polygonal and polyhedral domains," *IEEE Trans. Antennas Propagat.*, vol. 32, pp. 276–281, Mar. 1984.
- [26] Y. Oh, K. Sarabandi, and F. T. Ulaby, "An empirical model and an inversion technique for radar scattering from bare soil surfaces," *IEEE Trans. Geosci. Remote Sensing*, vol. 30, pp. 370–381, Mar. 1992.
- [27] L. Tsang and R. W. Newton, "Microwave emissions from soils with rough surfaces," *J. Geophys. Res.*, vol. 87, no. 11, pp. 9017–9024, Oct. 1982.
- [28] R. W. Newton, "Microwave remote sensing and its application to soil moisture detection," Remote Sensing Center, Texas A&M Univ., College Station, Tech. Rep. RSC-81, 1977.
- [29] R. W. Newton and J. W. Rouse, "Microwave radiometer measurements of soil moisture content," *IEEE Trans. Antennas Propagat.*, vol. AP-28, pp. 680–686, 1980.
- [30] T. J. Schmugge, T. Wilheit, W. Webster, Jr., and P. Gloersen, "Remote sensing of soil moisture with microwave radiometers," Goddard Space Flight Center, Greenbelt, MD, II, NASA TND-8321, 1976.
- [31] S. P. Durden and J. F. Vesecky, "A physical radar cross section model for a wind driven sea with swell," *IEEE J. Oceanic Eng.*, vol. OE-10, pp. 445–451, 1985.
- [32] S. H. Yueh, R. Kwok, F. K. Li, S. V. Nghiem, W. J. Wilson, and J. A. Kong, "Polarimetric passive remote sensing of ocean wind vectors," *Radio Sci.*, vol. 29, no. 4, pp. 799–814, July–Aug. 1994.
- [33] J. T. Johnson, J. A. Kong, R. T. Shin, S. H. Yueh, S. V. Nghiem, and R. Kwok, "Polarimetric thermal emission from rough ocean surfaces," *J. Electromagn. Waves Applicat.*, vol. 8, no. 1, pp. 43–59, 1994.
- [34] L. Zhou, L. Tsang, and D. Chen, "Polarimetric passive microwave remote sensing of wind vectors with foam covered rough ocean surfaces," *Radio Sci.*, vol. 38, no. 4, Aug. 2003.



Lin Zhou received the B.Eng. degree in electronic engineering from the University of Electronic Science and Technology, Chengdu, China, in 1989, the M.Eng. degree from National University of Singapore, in 1998, and the Ph.D. degree from the University of Washington, Seattle, in 2003.

Since September 2003, he has been with the department of Electrical and Computer Engineering, Duke University, Durham, NC, as a Research Associate. From 1989 to 1996, he was an Engineer with the Communications Division, Civil Aviation Administration of China. His current interests include computational electromagnetics and electron waveguide circuits.



Leung Tsang (S'73–M'75–SM'85–F'90) was born in Hong Kong. He received the S.B., S.M., and Ph.D. degrees from the Massachusetts Institute of Technology, Cambridge.

He is currently a Professor of electrical engineering at the University of Washington, Seattle, where he has taught since 1983. Starting September 2001, he has been on leave from the University of Washington and is a Professor Chair and Assistant Head of the Department of Electronic Engineering, the City University of Hong Kong. He is a coauthor

of four books: *Theory of Microwave Remote Sensing* (New York: Wiley-Interscience, 1985), *Scattering of Electromagnetic Waves, Vol. 1: Theory and Applications* (New York: Wiley-Interscience, 2000), *Scattering of Electromagnetic Waves, Vol. 2: Numerical Simulations* (New York: Wiley-Interscience, 2001), and *Scattering of Electromagnetic Waves, Vol. 3: Advanced Topics* (New York: Wiley-Interscience, 2001). His current research interests include wave propagation in random media and rough surfaces, remote sensing, high-speed interconnects, computational electromagnetics, wireless communications, and optoelectronics.

Dr. Tsang was Editor-in-Chief of the IEEE TRANSACTIONS ON GEOSCIENCE AND REMOTE SENSING. He was the Technical Program Chairman of the 1994 IEEE Antennas and Propagation International Symposium and URSI Radio Science Meeting, the Technical Program Chairman of the 1995 Progress in Electromagnetics Research Symposium, and the General Chairman of the 1998 IEEE International Geoscience and Remote Sensing Symposium. He is a Fellow of the Optical Society of America and the recipient of the Outstanding Service Award of the IEEE Geoscience and Remote Sensing Society for 2000. He was also a recipient of the IEEE Third Millennium Medal in 2000. He is also an AdCom member of the IEEE Geoscience and Remote Sensing Society.



Vikram Jandhyala (M'00–SM'03) received the B.Tech degree in electrical engineering from the Indian Institute of Technology, Delhi, in 1993, and the M.S. and Ph.D. degrees from the University of Illinois at Urbana-Champaign, in 1995 and 1998, respectively. As part of his graduate work, he codeveloped the steepest descent fast-multipole method for rapid simulation of a large class of electromagnetic problems.

From 1998 to 2000, he was a Research and Development Engineer at Ansoft Corporation, Pittsburgh, PA. He was involved in the acceleration of Ansoft's integral equation solvers and codeveloped a fast-multipole -based extraction tool in Ansoft's Spicelink versions released in 1999 and 2000. Since 2000, he has been an Assistant Professor in the Department of Electrical Engineering, University of Washington, Seattle. He directs the applied computational electromagnetics laboratory, with research interests and projects in several areas of computational electromagnetics, including fast solvers and integral equation formulations in frequency and time domains, high-speed circuits and devices, coupled multiphysics simulation, novel materials, and propagation. He has Visiting Research status at the Lawrence Livermore National Labs, is a recipient of an NSF CAREER grant in 2001, an Outstanding Graduate Research Award at the University of Illinois in 1998, and an IEEE Microwave Graduate Fellowship in 1996–1997). He has published more than 70 journal and conference articles.

Dr. Jandhyala has served as a reviewer for several IEEE journals and conferences and national and international proposal panels and is on the technical program committee of the IEEE Design Automation Conference and the IEEE Antennas and Propagation Symposium. He is a full elected member of URSI Commission B.

Qin Li received the B.S. and M.S. degrees in space physics from Wuhan University, Hubei, China, in 1985 and 1988, respectively, and the Ph.D. degree in electrical engineering from the University of Washington, Seattle, in 2000.

He is currently a Research Assistant Professor in the Department of Electrical Engineering, University of Washington. He has worked as a Post Graduate Researcher at the Institute for Computational Earth System Sciences, University of California, Santa Barbara.

Chi H. Chan (S'86–M'86–SM'00–F'02) received the Ph.D. degree in electrical engineering from the University of Illinois, Urbana, IL, in 1987.

From 1987 to 1989, he was a Visiting Assistant Professor in the Department of Electrical and Computer Engineering, University of Illinois. From 1989 to 1993, he was an Assistant Professor in the Electrical Engineering Department, University of Washington, Seattle. He became a tenured Associate Professor in 1993. In 1996, he joined the Department of Electronic Engineering, City University of Hong Kong, in April 1996, as a Professor and was promoted to Professor (Chair) of Electronic Engineering in 1998. He has been Associate Dean (Research) of the Faculty of Science and Engineering, City University of Hong Kong since 1998. He is also Guest Professor with the Xi'an Jiaotong University, Xi'an, China, and Wuhan University, Wuhan, China, and an Advisory Professor of Nanjing University of Science and Technology, Nanjing, China. His research focuses on computational electromagnetics and wireless communications.

Dr. Chan was a recipient of the 1991 U.S. National Science Foundation Presidential Young Investigator Award. He is a Fellow of the Chinese Institute of Electronics and the Institute of Electrical Engineers.